Analysis of Corona and Surface Discharge Signals from Different Non-Intrusive Sensors under HVDC

Ayyoub Zouaghi, Christian Vollaire, Matthieu Dalstein

▶ **To cite this version:**

Ayyoub Zouaghi, Christian Vollaire, Matthieu Dalstein. Analysis of Corona and Surface Discharge Signals from Different Non-Intrusive Sensors under HVDC. 2023 IEEE Industry Applications Society Annual Meeting (IAS), IEEE Industry Applications Society, Oct 2023, Nashville, United States. pp.1-5, 10.1109/IAS54024.2023.10406887 . hal-04460959

HAL Id: hal-04460959
https://hal.science/hal-04460959

Submitted on 12 Sep 2024

HAL is a multi-disciplinary open access archive for the deposit and dissemination of scientific research documents, whether they are published or not. The documents may come from teaching and research institutions in France or abroad, or from public or private research centers.

L'archive ouverte pluridisciplinaire **HAL**, est destinée au dépôt et à la diffusion de documents scientifiques de niveau recherche, publiés ou non, émanant des établissements d'enseignement et de recherche français ou étrangers, des laboratoires publics ou privés.

Analysis of corona and surface discharge signals from different non-intrusive sensors under HVDC

Ayyoub Zouaghi
Member, IEEE
Univ Lyon, Ecole Centrale de Lyon, INSA Lyon
Université Lyon 1, CNRS, Ampère, UMR5005, 69130
Ecully, France
ayyoub.zouaghi@ec-lyon.fr

Sneha Satish Hegde
Member, IEEE
Univ Lyon, Ecole Centrale de Lyon, INSA Lyon
Université Lyon 1, CNRS, Ampère, UMR5005, 69130
Ecully, France
sneha-satish.hegde@ec-lyon.fr

Christian Vollaire
Senior Member, IEEE
Univ Lyon, Ecole Centrale de Lyon, INSA Lyon
Université Lyon 1, CNRS, Ampère, UMR5005, 69130
Ecully, France
christian.vollaire@ec-lyon.fr

Matthieu Dalstein
SuperGrid Institute, 23 rue Cyprian, 69100
Villeurbanne, France
matthieu.dalstein@supergrid-institute.com

***Abstract*- The use of high voltage direct current (HVDC) transmission technology has increased significantly in recent years due to its numerous advantages over traditional alternating current (AC) transmission. The aim of the present work is to investigate the efficiency of different non-intrusive sensors for partial discharge measurement in medium or high voltage direct current equipment such as air or gas insulated switchgear. HV equipment are susceptible to partial discharges such as corona and surface discharges, which can lead to the premature aging of the insulation and its breakdown. The partial discharges appear because of the enhancement of the electric field around sharp edges, triple points, floating metallic particles or in cracks or cavities inside solid insulation. In HVAC systems, partial discharge detection and quantification are well understood. However, under HVDC, there is a necessity to evaluate the efficiency of classic techniques and commercial non-intrusive sensors. This work presents a study of three different sensors for partial discharge measurement under HVDC: high frequency current transformer (HFCT), ultra-high frequency antenna (UHF), and transient earth voltage (TEV). The signals of the different sensors partial discharge detection are presented and compared in both temporal and frequency domains.**

Keywords— partial discharge, high voltage, direct current, electric field, non-intrusive sensors, electric insulation, corona.

I. Introduction

In recent times, there has been a substantial uptick in the adoption of high voltage direct current (HVDC) transmission technology. This surge can be attributed to the manifold benefits it offers in comparison to the conventional method of alternating current (AC) transmission [1]. However, gas insulated HVDC systems are susceptible to partial discharges, including corona and surface discharges, which can lead to the premature aging of the insulation and its breakdown over time [2]–[4]. To prevent such occurrences, it is important to accurately monitor diagnosis and quantify the activity of these discharges. In the electric energy network, medium voltage (MV) and high voltage (HV) air or Gas Insulated Switchgears (GIS) are essential elements. In these equipment, the diagnosis and the monitoring of the degradation in the insulating system can be accomplished through Partial Discharge (PD) analysis [2], [5], [6].

In MV and HV gas insulated equipment, PDs occur as a result of the amplification of electric fields around pointed tips, edges, triple points, suspended metallic particles, surface pollution, or within fissures and voids present in solid insulation [7]. The presence of the partial discharges in the system produces electric current, electromagnetic waves, gas degradation, heat, and acoustic emissions [8]. As a consequence, there are multiple techniques that can be used to detect partial discharges efficiently, depending on the system and the desired information [9]–[12].

Non-intrusive sensors provide various advantages over conventional method for partial discharge (PD) detection described in IEC 60270 [13], including smaller size and the ability to monitor PD signals in real-time and real conditions without requiring direct contact with the insulation material. High Frequency Current Transformer (HFCT), Ultra-High Frequency (UHF) antenna, and Transient Earth Voltage (TEV) sensors are used to detect PD phenomena in different components in HVAC systems [12], [14], [15]. However, the efficiency of these techniques under HVDC conditions necessitates more investigation. In this work, these sensors are investigated to assess corona and surface discharges under HVDC in atmospheric pressure air. An analysis of the PD signals detected by the different non-intrusive sensors under HVDC is presented, with the aim of improving the understanding of these phenomena and developing effective monitoring strategies for HVDC systems. In addition to analyzing the signals generated by corona and surface discharges under HVDC, this paper focuses on studying the relation between the PD apparent charge and the maxima of the signals. Exploring different non-intrusive sensors and analyzing the signals they generate will be helpful to identify key features and patterns that can be used as reliable indicators of different default types, and improve the overall reliability and safety of HVDC transmission technology.

This work is presented in three sections, experimental setup section, results and discussion section, and a conclusion.

II. Experimental Setup

The experimental setup used for studding corona and surface discharges under HVDC systems is illustrated in Fig. 1. It is composed into two zones: the low voltage zone and the high voltage zone. In the low voltage zone, inputs such as the applied voltage amplitude are controlled, and the information from the sensors is acquired. The HV is generated using a HV amplifier (Matsusada AMP 20B20, 400 W, 20 kV) that is connected to the coupling capacitor (Omicron MCC 210L, 100 kV, 1 nF) and the device under test. The other three non-intrusive sensors, namely HFCT (bandwidth from 200 Hz-500 MHz), UHF

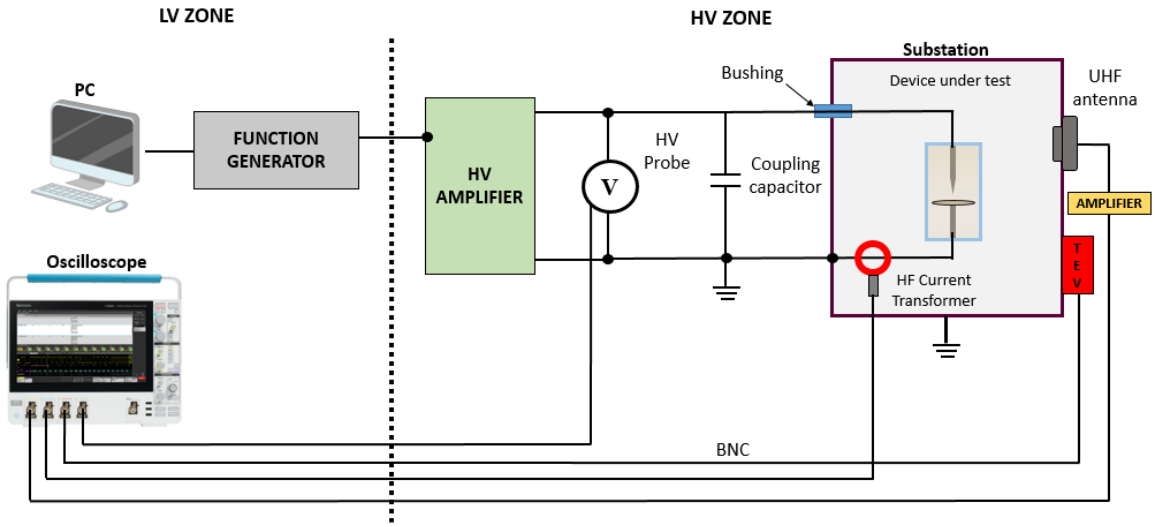

Fig. 1 Schematic diagram of the experimental setup

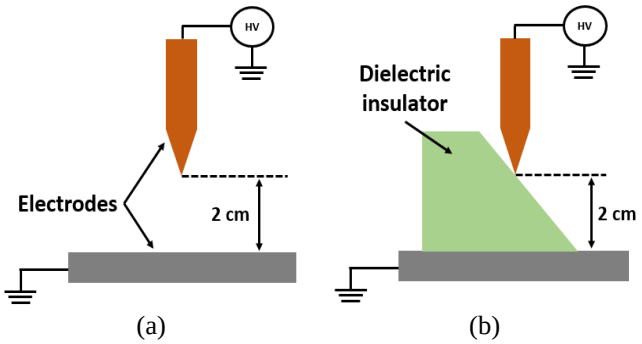

Fig. 2 Schematic illustrations of the two configurations. (a) Needle-plane corona, (b) surface discharge

antenna (up to 3 GHz), and TEV (up to 100 MHz), are connected across the sample under test to measure the PD activity. The oscilloscope (Tektronix MSO64, 6 GHz Bandwidth and 12.5 GS/s) displays the output generated by all the sensors.

The experiments are performed using two different configurations, namely needle-plane corona and surface discharge, following specific protocols. A schematic illustration of the two configurations is presented in Fig. 2. Corona discharge is produced using needle-plane configuration. The HV needle's tip has a radius of 200 µm. It is placed at a distance of 2 cm from a grounded plate electrode. The insulating material for the second configuration is made of PTFE and it is placed with an inclination angle of 45°. Prior to applying the voltage, pre-measurements are conducted at 0 V, and then the voltage is increased gradually and measurements are taken by applying voltage greater than the partial discharge inception voltage. The signals are then analyzed and processed using a Matlab code that was developed for this purpose. To minimize the noise and to mitigate signal disturbances, all the experimental setup and the measurement campaigns were conducted in an anechoic chamber.

III. Experimental Results

The PD signals recorded from the different sensors are analyzed in the time and frequency domain. The signals acquisition has been made at the same time. The applied voltage values are higher than the partial discharge inception voltage (PDIV) and lower than the breakdown voltage (BDV).

A. *I(V) curves*

Fig. 3 presents the evolution of the RMS value of the current as a function of the applied voltage for the needle-plane corona and surface discharge, with both positive and negative polarities. For the needle-plane corona, I(V) curves are in agreement with the literature [16]. They follow the Townsend empirical formula [17]: $I=C^{*}V(V-V_0)$, where V and V_0 are the applied DC voltage and the discharge onset voltage respectively and C a constant depending on the voltage polarity, electrode configuration, temperature, pressure and gas composition.

Negative polarity shows higher current values under 14 kV. For voltage amplitudes higher than 14 kV, the current in positive polarity becomes higher. This behavior can be attributed to the variation of the discharge mode, according to multiples authors [16], [18]–[20]. In fact, different positive corona discharge modes can be successively observed when the voltage amplitude goes up. In our case, a glow to streamer mode transition is observed. In the case of surface discharge configuration, we can see that when the dielectric insulator is added, the discharge inception voltage become very high compared to the first configuration. The current increases starting from 16 kV and 17 kV for the negative and positive polarities respectively. At 18.2 kV, the current under positive voltage becomes higher than that of the negative voltage which can be also attributed to the change of the discharge mode. In the following sections, our focus will be on the positive polarity.

Fig. 4 presents different discharge images of needle-plane corona and surface discharge under HVDC. The images show

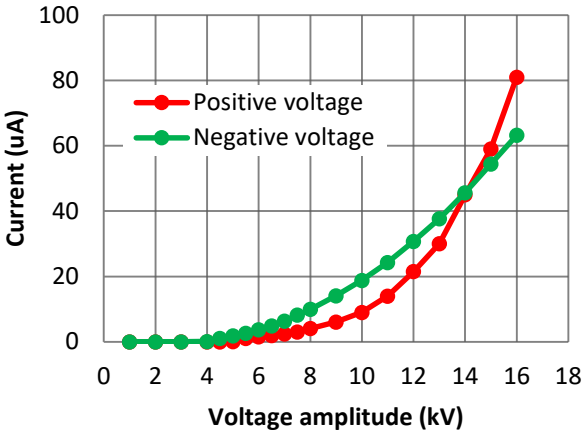

(a)

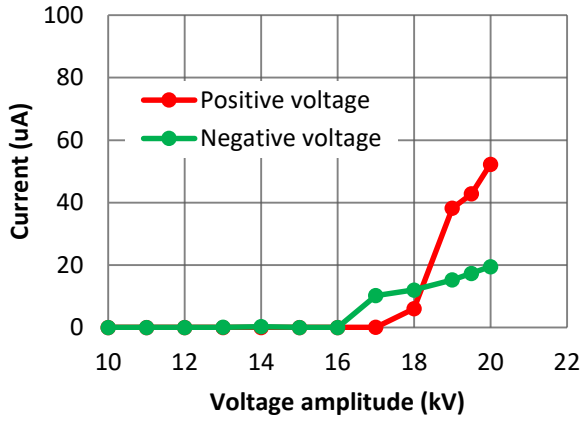

(b)

Fig. 3 Current-voltage characteristics under positive and negative applied voltage. (a) Needle-plane corona and (b) surface discharge configuration. T=24-29°C, H=30-40%

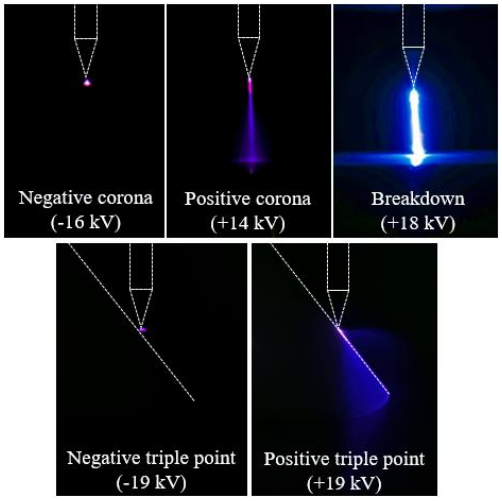

Fig. 4 Long exposure time discharge images under positive and negative DC applied voltage for needle-plane corona and surface discharge configuration. T=24-29°C, H=30-40%

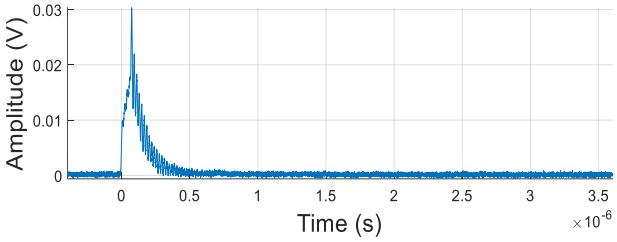

(a)

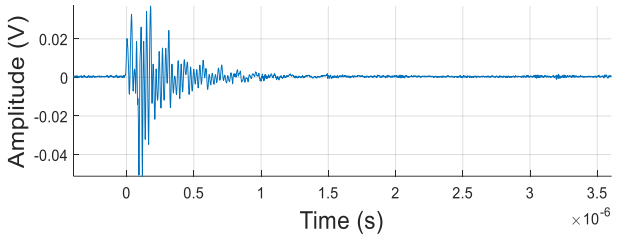

(b)

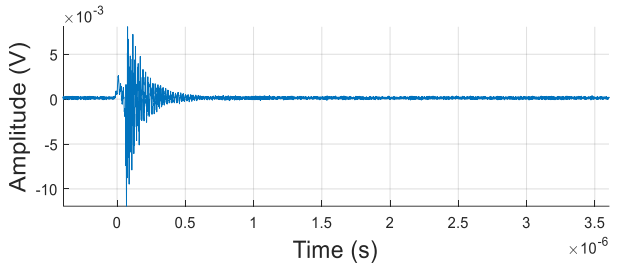

(c)

Fig. 5 Discharge pulses given by the three sensors under +14 kV for the needle-plane corona. (a) HFCT with 1A is equivalent to 1V, (b) TEV, (c) UHF. T=24-29°C, H=30-40%

different discharge modes for the discharges. Under negative polarity, one can observe a luminous area at the needle's tip indicating the discharge ignition. Under positive polarity, a streamer like mode can be observed where a luminous area is observed between the needle's tip and the grounded electrode. A similar observation can be made for the surface discharge configuration. The discharge modes observed are in agreement with the literature [16]. When the applied voltage is increased, a breakdown can take place. The PD signals from the different sensors have been recorded at voltage values higher than the PDIV and lower than the breakdown voltage (BDV).

B. Corona discharge signals

Fig. 5 presents the time evolution of one single discharge pulse signals given by the sensors HFCT, TEV and UHF over 3.5 µs under +14 kV. The signal given by the HFCT represents the image of the discharge current with an ampere to volt conversion ratio of 1. When the applied voltage reaches the PDIV value, electric charges are produced and migrated toward the grounded electrode. As a consequence, an electric current pulse is detected. The intensity and the repetition rate of these pulses increase with the voltage amplitude. These results clearly demonstrate the synchronization of PD pulses given by the three sensor. However, the pulse profiles are different. UHF antenna detects the electromagnetic waves produced by the

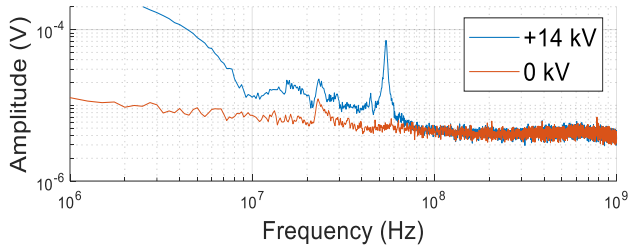

(a)

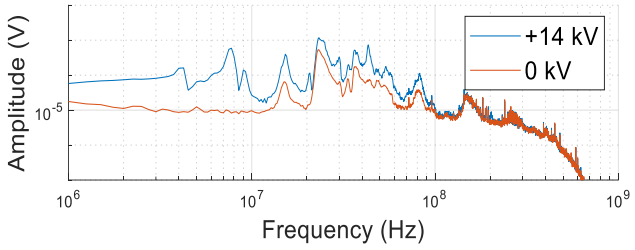

(b)

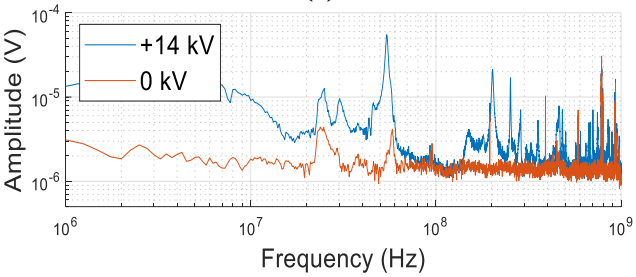

(c)

Fig. 6 FFT spectrum of the PD pulses of the three sensors under +14 kV for the needle-plane corona. (a) HFCT, (b) TEV, (c) UHF

partial discharge. These waves propagate inside the metallic enclosure and reach the antenna. On the other hand, TEV sensor signal intensity depends on the magnitude of the electromagnetic wave occurred due to PD activity and its time varying, the dielectric constant of capacitive parts in the TEV sensor, and the impedance of the metal wall [12].

C. FFT Spectrum

In this work, we are interested by analyzing the discharge signals of the three sensors in the frequency domain using Fast Fourier Transform (FFT). The results of this study are presented in Fig. 6. We can notice that the signals given by the three sensors show different FFT spectrums of one single pulse of the same PD. Under +14 kV, the FFT of the HFCT signal shows the presence of PD activity between 10 MHz and 70 MHz with the appearance of a peak at about 55 MHz. For the TEV sensor, we notice the presence of multiples peaks between 10 MHz and 100 MHz even at 0 kV. These peaks are caused by external perturbations coming essentially from the HV amplifier. When the high voltage is applied, one can notice the intensification of the previous peaks and the appearance of other ones under 10 MHz and at 20 MHz, 30 MHz and 45 MHz. For the UHF sensor, some peaks are also observable with the absence of PD because of the perturbations coming from the power supply. However, when the high voltage is applied, multiple new peaks appear at

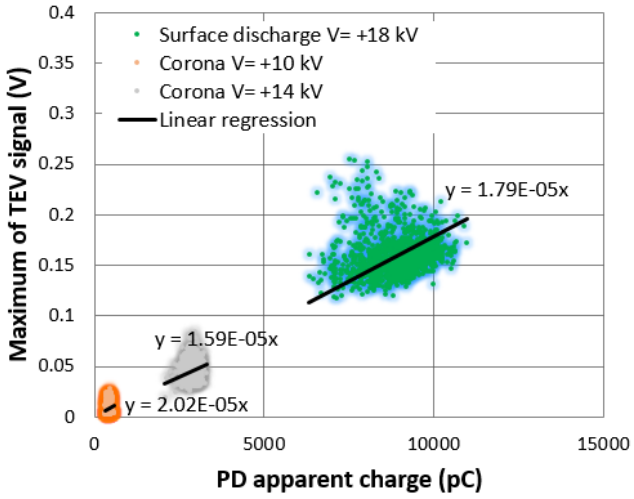

(a)

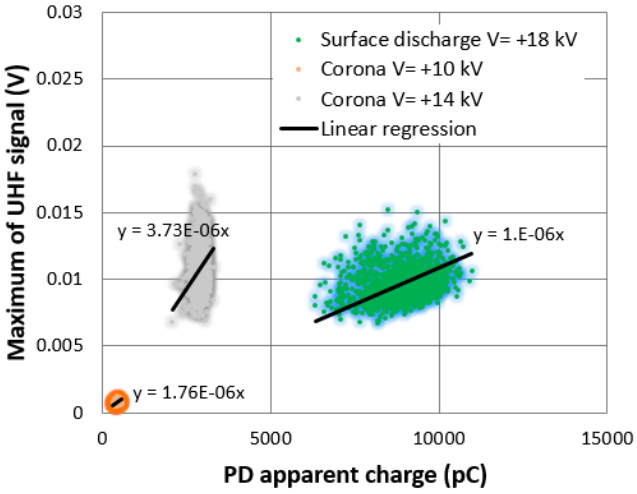

(b)

Fig. 7 Variation of the maxima of the pulses given by the sensors as a function of the apparent charge for needle-plane corona and surface discharge. (a) TEV sensor, (b) UHF antenna

the ultra-high frequency range, higher than 100 MHz, and also between 20 MHz and 60 MHz, which is the same frequency range as the HFCT. The difference of the frequency domain signature of the PD pulse of each sensor can be explained by the fact that each sensor measures different physical manifestation of the PD: electric current with HFCT, electromagnetic emissions with UHF and transient earth voltage with TEV, and the sensors don't have the same bandwidth.

D. Apparent charge

For PD diagnosis and monitoring, it is important to estimate the apparent charge of PD in Coulomb. Fig. 7 presents the variation of the maximum values of TEV and UHF signals as a function of the PD apparent charge for more than 1000 PD pulses. The PD apparent charge has been obtained by

integrating the current pulses over time, the values have been validated using the conventional method IEC 60270. This study will allow us to understand if the PD type and mode affect the maximum values of the signals coming from the non-intrusive sensors. Three cases have been studied, 10 kV and 14 kV positive needle-plane corona discharge and 18 kV positive surface discharge. The experimental observations have shown that the corona discharge mode is different for the two chosen applied voltage values. When the voltage increases, the apparent charge and the maximum values of the signals increase as well. For the TEV sensor, we can observe that the linear equation relating the maximum of the pulses and the apparent charge is nearly the same for the three studied cases. As a consequence, the TEV pulses maximum values are not dependent on the corona discharge mode nor on the PD type since nearly the same equation has been obtained also for corona and surface discharges. In the case of UHF sensor, different linear equations have been obtained between the maximum of the UHF PD pulses and their apparent charge. These results show that the maximum of the UHF PD pulses depends on the discharge mode as well as the discharge type.

IV. Conclusion

In this work, the effectiveness of various non-intrusive sensors for measuring partial discharges in MVDC and HVDC equipment, such as air or gas insulated switchgear is investigated. The PD has been analyzed using I(V) characteristics and the FFT of the PD pulses measured simultaneously by three different sensors. The results show that the PD pulses of the different sensors are synchronized. Since the different sensors measure different physical manifestations of the discharge: electric current with HFCT, electromagnetic emissions with UHF and transient earth voltage with TEV, the spectrum of the discharge pulses of each sensor is different. For HFCT, the PD pulse FFT shows discharge peaks mainly at the range from 10 MHz to 60 MHz. UHF antenna signal show pulses not only at the same frequency range as HFCT, but also at frequencies higher than 150 MHz. Otherwise, TEV sensor signal show more frequency content under 10 MHz. The measurements show also that the TEV sensor is more sensitive to external perturbations, multiple harmonics have been observed even without the discharge. The study of the apparent charge shows that the maxima of the TEV and UHF PD signals are depends on the apparent charge. However, the UHF signal depends also on the type and the mode of the discharge. The results of this paper will be helpful to better understand PD detection and monitoring using non-intrusive sensors under HVDC.

References

[1] M. P. Bahrman and B. K. Johnson, "The ABCs of HVDC transmission technologies," *IEEE Power Energy Mag.*, vol. 5, no. 2, pp. 32–44, Mar. 2007, doi: 10.1109/MPAE.2007.329194.

[2] T. Vu-Cong *et al.*, "Long-Term Partial Discharge Behavior of Protrusion Defect in HVDC GIS," *IEEE Trans. Dielectr. Electr. Insul.*, vol. 29, no. 6, pp. 2294–2302, Dec. 2022, doi: 10.1109/TDEI.2022.3206726.

[3] M. Florkowski, M. Kuniewski, and P. Zydroń, "Measurements and Analysis of Partial Discharges at HVDC Voltage with AC Components," *Energies*, vol. 15, no. 7, Art. no. 7, Jan. 2022, doi: 10.3390/en15072510.

[4] E. Ouss, A. Beroual, A. Girodet, G. Ortiz, L. Zavattoni, and T. Vu-Cong, "Characterization of partial discharges from a protrusion in HVDC coaxial geometry," *IEEE Trans. Dielectr. Electr. Insul.*, vol. 27, no. 1, pp. 148–155, Feb. 2020, doi: 10.1109/TDEI.2019.008359.

[5] R. Piccin, A. R. Mor, P. Morshuis, A. Girodet, and J. Smit, "Partial discharge analysis of gas insulated systems at high voltage AC and DC," *IEEE Trans. Dielectr. Electr. Insul.*, vol. 22, no. 1, pp. 218–228, Feb. 2015, doi: 10.1109/TDEI.2014.004711.

[6] C. Toigo, T. Vu-Cong, F. Jacquier, and A. Girodet, "Partial discharge behavior of protrusion on high voltage conductor in GIS/GIL under high voltage direct current: Comparison of SF6 and SF6 alternative gases," *IEEE Trans. Dielectr. Electr. Insul.*, vol. 27, no. 1, pp. 140–147, Feb. 2020, doi: 10.1109/TDEI.2019.008358.

[7] A. Rodrigo Mor, L. C. Castro Heredia, D. A. Harmsen, and F. A. Muñoz, "A new design of a test platform for testing multiple partial discharge sources," *Int. J. Electr. Power Energy Syst.*, vol. 94, pp. 374–384, Jan. 2018, doi: 10.1016/j.ijepes.2017.07.013.

[8] Y. Shibuya, S. Matsumoto, T. Konno, and K. Umezu, "Electromagnetic waves from partial discharges in windings and their detection by patch antenna," *IEEE Trans. Dielectr. Electr. Insul.*, vol. 18, no. 6, pp. 2013–2023, Dec. 2011, doi: 10.1109/TDEI.2011.6118639.

[9] A. Zouaghi, O. Agri, E. Vagnon, and J.-L. Auge, "Optical and Electrical Partial Discharge Measurement with A1N Dielectric Barrier in Mineral Oil," in *2020 IEEE Conference on Electrical Insulation and Dielectric Phenomena (CEIDP)*, Oct. 2020, pp. 243–246. doi: 10.1109/CEIDP49254.2020.9437536.

[10] H. D. Ilkhechi and M. H. Samimi, "Applications of the Acoustic Method in Partial Discharge Measurement: A Review," *IEEE Trans. Dielectr. Electr. Insul.*, vol. 28, no. 1, pp. 42–51, Feb. 2021, doi: 10.1109/TDEI.2020.008985.

[11] J. V. Klüss and A.-P. Elg, "Challenges Associated with Implementation of HFCTs for Partial Discharge Measurements," in *2020 Conference on Precision Electromagnetic Measurements (CPEM)*, Aug. 2020, pp. 1–2. doi: 10.1109/CPEM49742.2020.9191781.

[12] H. Prasetia, U. Khayam, Suwarno, A. Itose, M. Kozako, and M. Hikita, "PD pattern of various defects measured by TEV sensor," in *2017 International Conference on High Voltage Engineering and Power Systems (ICHVEPS)*, Oct. 2017, pp. 23–28. doi: 10.1109/ICHVEPS.2017.8225861.

[13] High-voltage test techniques – Partial discharge measurements, IEC 60270:2000.

[14] S. Tenbohlen *et al.*, "Frequency Range of UHF PD Measurements in Power Transformers," *Energies*, vol. 16, no. 3, Art. no. 3, Jan. 2023, doi: 10.3390/en16031395.

[15] A. Loubani, N. Harid, H. Griffiths, and B. Barkat, "Simulation of Partial Discharge Induced EM Waves Using FDTD Method—A Parametric Study," *Energies*, vol. 12, no. 17, p. 3364, Sep. 2019, doi: 10.3390/en12173364.

[16] E. Moreau, P. Audier, and N. Benard, "Ionic wind produced by positive and negative corona discharges in air," *J. Electrost.*, vol. 93, pp. 85–96, Jun. 2018, doi: 10.1016/j.elstat.2018.03.009.

[17] J. S. Townsend and P. J. Edmunds, "LXXXIX. The discharge of electricity from cylinders and points," *Lond. Edinb. Dublin Philos. Mag. J. Sci.*, vol. 27, no. 161, pp. 789–801, May 1914, doi: 10.1080/14786440508635151.

[18] L. B. Loeb and A. F. Kip, "Electrical Discharges in Air at Atmospheric Pressure The Nature of the Positive and Negative Point-to-Plane Coronas and the Mechanism of Spark Propagation," *J. Appl. Phys.*, vol. 10, no. 3, pp. 142–160, Mar. 1939, doi: 10.1063/1.1707290.

[19] W. N. English, "Positive and Negative Point-to-Plane Corona in Air," *Phys. Rev.*, vol. 74, no. 2, pp. 170–178, Jul. 1948, doi: 10.1103/PhysRev.74.170.

[20] T. N. Giao and J. B. Jordan, "Modes of Corona Discharges in Air," *IEEE Trans. Power Appar. Syst.*, vol. PAS-87, no. 5, pp. 1207–1215, May 1968, doi: 10.1109/TPAS.1968.292211.